First Rb Silicotitanate Phase and Its K-Structural Analogue: New Members of the SNL-A Family (*Cc*-$A_2TiSi_6O_{15}$; A = K, Rb, Cs)

M. Nyman,[†] F. Bonhomme,[†] R. S. Maxwell,[‡] and T. M. Nenoff*[,†]

Sandia National Laboratories, Department 6233, P.O. Box 8500 M.S. 0755, Albuquerque, New Mexico 87185-0755, and Lawrence Livermore National Laboratory, Analytical and Nuclear Sciences Division, P.O. Box 808/L-091, Livermore, California 94551

Received April 11, 2001. Revised Manuscript Received September 12, 2001

Alkali silicotitanate ternary phases have been studied for a wide variety of applications including catalysis, selective ion exchange, and ceramic nuclear waste form materials. We report here the synthesis and structural characterization of $Rb_2TiSi_6O_{15}$ and $K_2TiSi_6O_{15}$, structural analogues to SNL-A (*Cc*-$Cs_2TiSi_6O_{15}$). The Rb analogue is the first reported ternary oxide, the rubidium silicotitanate phase. Both the Rb and the K analogues were synthesized nearly pure by hydrothermal treatment of oxide precursor mixtures seeded with SNL-A and could not be synthesized without the addition of the seed. Rietveld refinement gave good structural models in the *Cc* space group with unit cell parameters: $Rb_2TiSi_6O_{15}$, $V = 1357.9$ Å^3, $a = 12.736(2)$ Å, $b = 7.3392(3)$ Å, $c = 15.061(3)$ Å, $\beta = 105.29(2)°$ and $K_2TiSi_6O_{15}$, $V = 1318.5$ Å^3, $a = 12.570(2)$ Å, $b = 7.2534(3)$ Å, $c = 15.082(3)$ Å, $\beta = 106.49(3)°$. The two isostructural phases were also characterized by thermogravimetry and ^{29}Si NMR. Unit cell parameters, melting temperatures, and ^{29}Si chemical shifts were compared to those of the Cs analogue and related to variation in alkali radius (Cs > Rb > K). The volume, the *a*-axis, and the *b*-axis increase linearly with alkali radius, which is directly related to a "relaxation" of the folds of the corrugated silicate layers that lie in the *xy* plane.

Introduction

Open-framework, microporous silicotitanate materials containing four-, five-, and six-coordinate titanium have received much ongoing attention for their technologically relevant properties, specifically catalysis and ion exchange.[1−19] For instance, silicotitanates that contain dopant levels (<5%) of titanium (four coordinate) substituted into a tetrahedral silicon site have excellent reactivity and selectivity toward epoxidation of olefins.[4,12] Five-coordinate titanium in silicotitanate JDF-L1 also exhibits catalytic behavior.[16] Furthermore, silicotitanates with stoichiometric concentrations of octahedrally coordinated titanium (six coordinate) in the framework are excellent ion exchangers with desirable properties such as high selectivity, high chemical and thermal stability, or high ion-exchange capacity. Examples of these materials include a silicotitanate analogue of pharmacosiderite and crystalline silicotitanate (CST).[1,2,14]

While microporous silicotitanate phases are studied extensively for environmental and industrial applications, their condensed phase counterparts[20−22] have not received nearly as much attention. We are interested in the discovery and characterization of new condensed silicotitanate phases to expand the knowledge base for this class of materials. These materials are potential condensed ceramic waste form phases for their related microporous ion exchanger phases,[20] especially for

* To whom correspondence should be addressed. E-mail: tmnenof@sandia.gov.
[†] Sandia National Laboratories.
[‡] Lawrence Livermore National Laboratory.

(1) Anthony, R. G.; Phillip, C. V.; Dosch, R. G. *Waste Manage. (Oxford)* **1993**, *13*, 503.
(2) Behrens, E. A.; Poojary, D. M.; Clearfield, A. *Chem. Mater.* **1994**, *8*, 1236.
(3) Chapman, D. M.; Roe, A. L. *Zeolites* **1990**, *10*, 730.
(4) Corma, A.; Garcia, H.; Navarro, M. T.; Palomares, E. J.; Rey, F. *Chem. Mater.* **2000**, *12*, 3068.
(5) Dadachov, M. S.; Rocha, J.; Ferreira, A.; Lin, Z.; Anderson, M. W. *J. Chem. Soc., Chem. Commun.* **1997**, 2371.
(6) Dadachov, M. S.; LeBail, A. *Eur. J. Solid State Inorg. Chem.* **1997**, *34*, 381.
(7) Dartt, C. B.; Davis, M. E. *Appl. Catal., A* **1996**, *143*, 53.
(8) Das, T. K.; Chandwadkar, A. J.; Sivasanker, S. *J. Chem. Soc., Chem. Commun.* **1996**, 1105.
(9) Du, H.; Fang, M.; Chen, J.; Pang, W. *J. Mater. Chem.* **1996**, *6*, 1827.
(10) Kuznicki, S. M. Preparation of small-pored crystalline titanium molecular sieve zeolites, U.S. Patent 4,938, 939, 1990.
(11) Liu, X.; Thomas, J. K. *J. Chem. Soc., Chem. Commun.* **1996**, 1435.
(12) Notari, B. *Adv. Catal.* **1996**, *41*, 253.
(13) Nyman, M.; Gu, B. X.; Wang, L. M.; Ewing, R. C.; Nenoff, T. M. *Microporous Mesoporous Mater.* **2000**, *40*, 115.
(14) Poojary, D. M.; Cahill, R. A.; Clearfield, A. *Chem. Mater.* **1994**, *6*, 2364.
(15) Reddy, J. S.; Kumar, R.; Ratnasamy, P. *Appl. Catal.* **1990**, *L1*, 58.
(16) Roberts, M. A.; Sankar, G.; Thomas, J. M.; Jones, R. H.; Du, H.; Chen, J.; Pang, W.; Su, R. *Nature* **1996**, *381*, 401.
(17) Rocha, J.; Anderson, M. W. *Eur. J. Inorg. Chem.* **2000**, *6*, 801.
(18) Serralha, F. N.; Lopes, J. M.; Lemos, F.; Prazeres, D.; Aires-Barros, M.; Rocha, J.; Cabral, J.; Riberiro, F. R. *React. Kinet. Catal. Lett.* **2000**, *2*, 217.
(19) Wang, X.; Guo, X. *Catal. Today* **1999**, *51*, 177.
(20) Nyman, M.; Bonhomme, F.; Teter, D. M.; Maxwell, R. S.; Gu, B. X.; Wang, L. M.; Ewing, R. C.; Nenoff, T. M. *Chem. Mater.* **2000**, *12*, 3449.
(21) Su, Y.; Balmer, M. L.; Bunker, B. C. *J. Phys. Chem. B* **2000**, *104*, 8160 (and references therein).
(22) Labouriau, A.; Higley, T. J.; Earl, W. L. *J. Phys. Chem. B* **1998**, *102*, 2897 and references therein.

10.1021/cm0102943 CCC: $20.00
Published on Web 11/03/2001

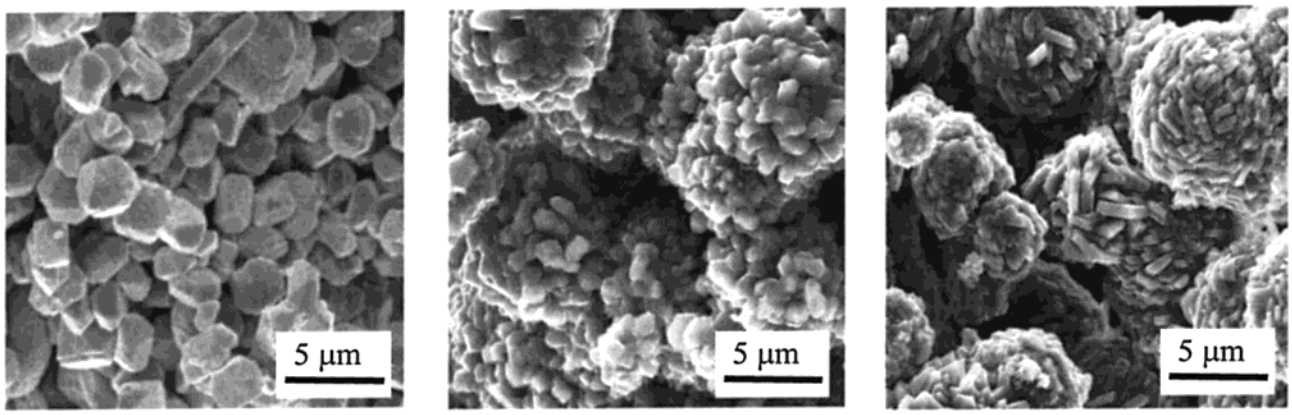

Figure 1. SEM images of structural analogues: (a) $Cs_2TiSi_6O_{15}$, (b) $Rb_2TiSi_6O_{15}$, and (c) $K_2TiSi_6O_{15}$.

sequestration and immobilization of radionuclides from mixed nuclear wastes.[23] Silicotitanate frameworks as ceramic waste forms are of particular interest due to their durability in chemical and radiation environments.[20,24,25] In pursuit of this application, we are currently investigating the stability of condensed silicotitanate phases as a function of composition and structure.

Recently, we reported hydrothermal synthesis, structural characterization, and chemical and radiation stability of SNL-A (*Cc*-space group $Cs_2TiSi_6O_{15}$), a highly stable, condensed silicotitanate phase.[20] Initially, analogous hydrothermal synthesis reactions using aqueous A-Si-Ti (A = Rb, K) oxide/hydroxide precursor mixtures yielded only amorphous products. However, seeding these mixtures with SNL-A resulted in the precipitation of nearly phase pure rubidium and potassium structural analogues of SNL-A. More importantly, the Rb analogue is the first reported $Rb_2O/TiO_2/SiO_2$ ternary oxide phase.

In addition to the Cs, Rb, and K phases which are the subject of this report, we have also synthesized mixed alkali phases, $(A_xA'_{1-x})_2TiSi_6O_{15}$ (A, A′ = Na, K, Rb, Cs), thus forming an entire family of isostructural silicotitanates. A future report on these materials will include calorimetry and structural studies on the family of the phases, to correlate structure and thermodynamic stability with composition.[26] The focus of the current work includes: (1) Synthesis of well-crystallized and highly pure $Rb_2TiSi_6O_{15}$ and $K_2TiSi_6O_{15}$ end members of this family of materials by seeding methods, (2) characterization by Rietveld refinement, differential thermal analysis (DTA), and ^{29}Si Magic Angle Spinning (MAS) NMR spectroscopy, and (3) comparison of structural features of $Cs_2TiSi_6O_{15}$, $Rb_2TiSi_6O_{15}$, and $K_2TiSi_6O_{15}$, especially with regard to the effect of the conformation of the corrugated silicate layers on the unit cell dimensions.

Experimental Section

General Instrumentation. The X-ray powder diffraction (XRD) patterns of $Rb_2TiSi_6O_{15}$ and $K_2TiSi_6O_{15}$ were measured on a Siemens D500 diffractometer with Ni-filtered Cu Kα radiation. The data were collected over the angular range of

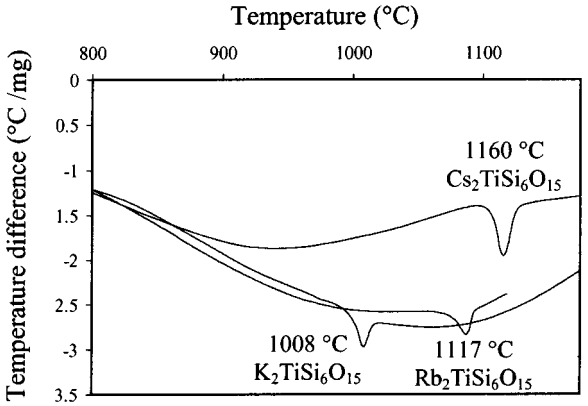

Figure 2. Differential thermal analysis spectra comparing melting temperatures of $Cs_2TiSi_6O_{15}$, $Rb_2TiSi_6O_{15}$, and $K_2TiSi_6O_{15}$.

Table 1. Crystallographic Data for $Rb_2TiSi_6O_{15}$ and $K_2TiSi_6O_{15}$

chemical formula	$Rb_2TiSi_6O_{15}$	$K_2TiSi_6O_{15}$
molar mass (g mol^{-1})	627.5	534.7
crystal system	monoclinic	monoclinic
space group	*Cc* (#9)	*Cc* (#9)
a (Å)	12.736(2)	12.570(2)
b (Å)	7.3392(3)	7.2534(3)
c (Å)	15.061(3)	15.082(3)
β (deg)	105.29(2)	106.49(3)
volume (Å^3)	1357.9(6)	1318.5(6)
Z	4	4
d_c (g cm^{-3})	3.07	2.69
λ	Cu Kα$_1$, Kα$_2$	Cu Kα$_1$, Kα$_2$
geometry	Bragg−Brentano	Bragg−Brentano
range 2*θ* (deg)	5.00−90.00	5.00−90.00
step size (deg)	0.04	0.04
time per step (s)	60	40
no. of free params	91[a]	91[a]
no. of structural params	74[b]	74[b]
no. of reflections	552	537
no. of soft constraints	66[ψ]	66[ψ]
minimum fwhm (deg)	0.13	0.10
R_{Bragg} (%)	3.73	4.35
R_{wp} (%)	10.31	14.49
R_{exp} (%)	2.93	3.75
χ^2	12.37	14.94

[a] 74 structural parameters plus 17 profile parameters (cell parameters, pseudo-Voigt mixing parameter, background, asymmetry, etc.). [b] 70 positional parameters (*x*, *y*, *z*) plus four isotropic temperature factors; 24 Si−O bond distance constraints (1.60 ± 0.01 Å); 6 Ti−O bond distance constraints (1.94 ± 0.025 Å); 36 O−Si−O angle constraints (109.5° ± 1.0°).

(23) Vance, E. R. *J. Mater. Sci.* **1986**, *21*, 1413.
(24) Su, Y.; Balmer, M. L.; Bunker, B. C. *Evaluation of Cesium Silicotitanates as an Alternative Waste Form*; Boston, MA, 1997; 457.
(25) Su, Y.; Balmer, M. L.; Wang, L.; Bunker, B. C.; Nenoff, T. M.; Nyman, M.; Navrotsky, A. *Evaluation of Thermally Converted Silicotitanate Waste Forms*; Boston, MA, 1998; 77.
(26) Nyman, M.; Nenoff, T. M.; Xu, H.; Navrotsky, A. In preparation.

Table 2. Structural Parameters for $Rb_2TiSi_6O_{15}$ and $K_2TiSi_6O_{15}$

	$Rb_2TiSi_6O_{15}$[a]			$K_2TiSi_6O_{15}$[a]		
atom	*x* (esd)	*y* (esd)	*z* (esd)	*x* (esd)	*y* (esd)	*z* (esd)
A1 (A = Rb, K)[c]	0.2597	0.3753(6)	0.4815	0.2597	0.426(1)	0.4815
A2 (A = Rb, K)	0.2779(4)	0.1361(6)	0.8077(3)	0.296(1)	0.176(1)	0.7921(7)
Ti	0.5528(7)	0.2396(8)	0.4048(6)	0.5471(1)	0.250(1)	0.3675(8)
Si1	−0.0043(7)	0.077(1)	0.2540(7)	−0.021(1)	0.047(1)	0.1994(7)
Si2	0.0459(7)	0.027(1)	0.5669(6)	0.022(1)	0.069(1)	0.5110(8)
Si3	0.0852(7)	0.451(1)	0.2445(6)	0.087(1)	0.410(1)	0.2301(8)
Si4	0.2568(7)	0.098(1)	0.0561(6)	0.249(1)	0.051(1)	0.0255(8)
Si5	0.3176(7)	0.319(1)	0.2447(7)	0.313(1)	0.279(1)	0.2120(8)
Si6	0.4811(7)	0.068(1)	0.0347(7)	0.480(1)	0.022(1)	0.0266(8)
O1	−0.008(1)	0.138(2)	0.0009(9)	−0.022(2)	0.049(2)	−0.082(1)
O2	−0.001(1)	0.298(1)	0.264(1)	−0.004(2)	0.258(2)	0.236(1)
O3	0.052(1)	0.505(2)	0.1388(8)	0.047(1)	0.516(2)	0.1338(9)
O4	0.047(1)	0.014(2)	0.1722(8)	−0.011(2)	0.031(2)	0.095(1)
O5	0.1710(9)	0.058(2)	0.564(1)	0.156(1)	0.095(2)	0.536(1)
O6	0.2025(9)	0.350(2)	0.269(1)	0.198(1)	0.298(2)	0.237(1)
O7	0.301(1)	0.199(2)	0.1539(9)	0.286(2)	0.171(2)	0.117(1)
O8	0.3558(9)	0.002(2)	0.025(1)	0.357(1)	−0.060(2)	0.013(1)
O9	0.369(1)	0.517(2)	0.230(1)	0.357(1)	0.483(2)	0.198(1)
O10	0.396(1)	0.223(2)	0.330(1)	0.402(1)	0.172(2)	0.292(1)
O11	0.479(1)	0.289(1)	0.034(1)	0.466(1)	0.231(2)	−0.007(1)
O12	0.528(1)	0.014(2)	0.461(1)	0.544(1)	0.091(2)	0.468(1)
O13	0.558(1)	0.484(2)	0.3462(8)	0.567(1)	0.414(2)	0.267(1)
O14	0.590(1)	0.118(2)	0.3092(1)	0.612(1)	0.046(2)	0.316(1)
O15	0.700(1)	0.261(2)	0.478(1)	0.698(1)	0.319(2)	0.439(1)

[a] $K_2TiSi_6O_{15}$: B_{iso}(K) = 5.3(2); B_{iso}(Ti) = 4.4(2); B_{iso}(Si) = 5.5(1); B_{iso}(O) = 4.2(2). [b] $Rb_2TiSi_6O_{15}$: B_{iso}(Rb) = 5.3(1); B_{iso}(Ti) = 3.2(2); B_{iso}(Si) = 3.9(1); B_{iso}(O) = 3.8(1). [c] *x* and *z* of A1 are fixed because *a* and *c* are origin-free directions in *Cc*.

Table 3. Selected Bond Angles (deg) and Distances (Å) for $Rb_2TiSi_6O_{15}$

atom	$O(x)_1$	A−$O(x)_1$ bond (length (Å) (esd)	$O(x)_2$	$O(x)_1$−A−$O(x)_2$ bond angle (deg) (esd)	atom	$O(x)_1$	A−$O(x)_1$ bond length (Å) (esd)	$O(x)_2$	$O(x)_1$−A−$O(x)_2$ bond angle (deg) (esd)
Ti	O1	1.99(1)	O10	87.4(0.7)	Si3	O2	1.625(8)	O3	110.5(0.7)
	O10	1.96(1)	O12	88.4(0.7)		O3	1.594(8)	O6	109.4(0.7)
	O12	1.91(1)	O14	91.6(0.7)		O6	1.607(8)	O14	108.7(0.7)
	O13	2.01(1)	O14	90.9(0.7)		O14	1.588(8)	O2	110.3(0.7)
	O14	1.89(1)	O15	90.9(0.7)		O2		O6	107.3(0.7)
	O15	1.97(1)	O1	92.6(0.7)		O3		O14	110.6(0.7)
	O1		O12	87.6(0.7)	Si4	O7	1.609(8)	O8	110.7(0.6)
	O1		O13	89.7(0.7)		O8	1.616(8)	O5	108.4(0.6)
	O10		O13	88.9(0.7)		O5	1.608(8)	O15	109.3(0.7)
	O10		O14	88.3(0.7)		O15	1.593(9)	O7	110.5(0.7)
	O12		O15	92.5(0.7)		O7		O5	110.0(0.7)
	O13		O15	90.1(0.7)		O8		O15	107.8(1.9)
Si1	O2	1.621(8)	O4	110.6(0.7)	Si5	O6	1.615(8)	O7	110.7(0.7)
	O4	1.607(8)	O9	109.6(0.7)		O7	1.599(8)	O9	110.1(0.7)
	O9	1.617(8)	O13	108.7(0.7)		O9	1.626(8)	O10	108.5(0.7)
	O13	1.578(9)	O2	110.8(0.7)		O10	1.585(8)	O6	106.9(0.7)
	O2		O9	107.2(0.6)		O6		O9	109.2(0.7)
	O13		O4	109.9(0.7)		O7		O10	111.4(0.7)
Si2	O5	1.617(8)	O11	108.5(0.7)	Si6	O8	1.620(8)	O11	107.1(0.6)
	O11	1.603(8)	O1	109.9(0.7)		O11	1.618(8)	O3	109.8(0.7)
	O1	1.601(8)	O4	110.9(0.7)		O3	1.597(8)	O12	110.9(0.7)
	O4	1.610(9)	O5	107.2(0.7)		O12	1.582(9)	O8	109.4(0.7)
	O5		O1	110.8(0.7)		O8		O3	109.8(0.7)
	O11		O4	109.4(0.7)		O11		O12	109.8(0.7)

Rb−O Distances (Å)

Rb1	O(*x*)	distance	O(*x*)	distance	Rb2	O(*x*)	distance	O(*x*)	distance
	O1	2.89(1)	O9	3.72(2)		O2	3.09(1)	O9	3.15(1)
	O2	3.10(1)	O10	3.39(2)		O4	3.29(1)	O10	3.01(1)
	O5	3.00(1)	O11	3.66(1)		O5	3.61(1)	O11	3.85(1)
	O6	3.09(1)	O12	3.06(2)		O6	3.89(1)	O12	3.58(2)
	O8	3.03(1)	O14	3.41(1)		O7	3.45(1)	O13	3.12(2)
			O15	2.92(1)		O8	3.31(1)	O14	3.00(2)
								O15	3.09(2)

5−100° 2θ with a step size of 0.04° and a counting time of 40 and 60 s per step, respectively. The front-loaded samples were rotated at 30 rpm during the measurement. The ^{29}Si MAS NMR spectrometry was performed at 99.4 MHz on a Bruker DRX-500 spectrometer and 4 mm CPMAS probe. The ^{29}Si MAS NMR spectra were obtained with 1-pulse acquire experiments though full nonselective with $\pi/2$ pulses of 8.5 μs. Neat tetramethylsilane (TMS) was used as an external standard (0 ppm) for the ^{29}Si NMR. A recycle delay of 600 s was used, and 400 scans each were collected. Differential thermal analysis−thermogravimetric analysis (DTA−TGA) experiments were performed on a STD 2960 TA DTA−TGA instrument with alumina as a standard for DTA. Samples (10−15 mg) were heated at 10 °C min^{-1} to 1200 °C and cooled back to ambient

Table 4. Selected Bond Angles (deg) and Distances (Å) for $K_2TiSi_6O_{15}$

atom	$O(x)_1$	A−$O(x)_1$ bond length (Å) (esd)	$O(x)_2$	$O(x)_1$−A−$O(x)_2$ bond angle (deg) (esd)	atom	$O(x)_1$	A−$O(x)_1$ bond length (Å) (esd)	$O(x)_2$	$O(x)_1$−A−$O(x)_2$ bond angle (deg) (esd)
Ti	O1	1.96(1)	O10	89.9(0.9)	Si3	O2	1.607(9)	O3	110.0(0.7)
	O10	1.95(1)	O12	93.5(0.7)		O3	1.594(8)	O6	110.4(0.7)
	O12	1.91(1)	O14	87.7(0.8)		O6	1.595(8)	O14	106.7(0.7)
	O13	2.00(1)	O14	89.5(0.8)		O14	1.583(9)	O2	111.3(0.7)
	O14	1.96(1)	O15	87.8(0.7)		O2		O6	105.6(0.7)
	O15	1.96(1)	O1	94.0(0.8)		O3		O14	112.5(0.7)
	O1		O12	92.0(0.9)	Si4	O7	1.592(8)	O8	109.3(0.7)
	O1		O13	90.9(0.7)		O8	1.632(9)	O5	110.2(0.7)
	O10		O13	91.6(0.7)		O5	1.623(8)	O15	109.3(0.7)
	O10		O14	88.3(0.8)		O15	1.595(9)	O7	109.8(0.7)
	O12		O15	87.5(0.8)		O7		O5	107.9(0.7)
	O13		O15	87.2(0.8)		O8		O15	110.4(0.7)
Si1	O2	1.619(9)	O4	111.4(0.7)	Si5	O6	1.601(8)	O7	106.5(0.7)
	O4	1.621(8)	O9	108.0(0.7)		O7	1.581(8)	O9	109.5(0.7)
	O9	1.602(9)	O13	108.8(0.7)		O9	1.612(9)	O10	110.5(0.8)
	O13	1.601(9)	O2	110.5(0.7)		O10	1.595(9)	O6	110.6(0.7)
	O2		O9	108.1(0.7)		O6		O9	108.4(0.7)
	O13		O4	110.1(0.7)		O7		O10	111.3(0.7)
Si2	O5	1.623(9)	O11	108.1(0.7)	Si6	O8	1.615(9)	O11	106.8(0.7)
	O11	1.605(9)	O1	107.5(0.7)		O11	1.595(9)	O3	109.3(0.7)
	O1	1.604(9)	O4	110.5(0.7)		O3	1.596(8)	O12	110.7(0.7)
	O4	1.612(8)	O5	110.6(0.7)		O12	1.583(9)	O8	110.7(0.7)
	O5		O1	110.1(0.7)		O8		O3	109.4(0.7)
	O11		O4	110.0(0.7)		O11		O12	109.9(0.7)

K−O Distances (Å)

K1	O(*x*)	distance	O(*x*)	distance	K2	O(*x*)	distance	O(*x*)	distance
	O1	3.16(2)	O9	3.22(2)		O1	3.70(2)	O9	3.05(2)
	O4	2.92(2)	O10	3.91(2)		O2	2.91(2)	O10	2.85(2)
	O5	2.96(2)	O11	3.56(2)		O5	3.40(3)	O11	3.19(2)
	O6	3.66(2)	O12	2.91(2)		O6	3.67(1)	O12	3.97(2)
	O7	3.53(2)	O14	2.79(2)		O7	3.62(2)	O13	2.86(2)
	O8	2.91(2)	O15	2.97(2)		O8	3.62(2)	O14	3.16(2)
								O15	2.81(2)

temperature at the same rate. Argon was used as a sweep gas with a flow of 20 cm^3 min^{-1}. Scanning electron microscopy (SEM) data were collected on a JEOL JSM-T300 SEM with energy dispersive (EDS) capabilities. Samples were mounted on a graphite disk and either carbon-coated (for EDS analysis) or gold-coated (for images).

Synthesis. *$Rb_2TiSi_6O_{15}$*. Titanium isopropoxide (Aldrich 99.999% purity TIPT, 0.235 g, 0.83 mmol) and tetraethyl orthosilicate (ACROS, 98% purity TEOS, 1.03 g, 4.95 mmol) were combined by stirring and added dropwise to a mixture of DI H_2O (4 mL), 50 wt % RbOH solution (Aldrich 99% purity, 0.51 g, 2.5 mmol), and 0.0075 g of $Cs_2TiSi_6O_{15}$20 (as a seed for crystal growth) in a 23 mL Teflon liner of a Parr pressure reactor. After the mixture was stirred for approximately 30 min, an additional 4 mL of H_2O was added and the mixture was stirred for 30 min more. The final pH of the mixture was approximately 11.8 with a final stoichiometry of Rb/Ti/Si/H_2O = 3:1:6:535. The Parr pressure reactor was placed in a 230 °C oven and heated for 4 weeks. The microcrystalline powder product was collected by filtration and rinsed with DI H_2O. Yield: 0.46 g (88%, based on TIPT).

$K_2TiSi_6O_{15}$. Titanium isopropoxide (Aldrich 99.999% purity TIPT, 0.235 g, 0.83 mmol) and tetraethyl orthosilicate (ACROS 98% purity TEOS, 1.03 g, 4.95 mmol) were combined by stirring and added dropwise to a mixture of DI H_2O (4 mL), KOH (Fisher reagent grade, 0.14 g, 2.5 mmol) and 0.0075 g of $Cs_2TiSi_6O_{15}$[20] (as a seed for crystal growth) in a 23 mL Teflon liner of a Parr pressure reactor. After the mixture was stirred for approximately 30 min, an additional 4 mL of H_2O was added and the mixture was stirred for 30 min more. The final pH of the mixture was approximately 11.4 with a final stoichiometry of K/Ti/Si/H_2O = 3:1:6:535. The Parr pressure reactor was placed in a 230 °C oven and heated for 3 days. The microcrystalline powder product was collected by filtration and rinsed with DI H_2O. Yield: 0.41 g (93%, based on TIPT).

Results and Discussions

Synthesis. Both rubidium and potassium analogues of SNL-A ($Cs_2TiSi_6O_{15}$)[20] could not be synthesized without seeding the synthesis reactions with SNL-A. Initial attempts produced only amorphous products or a poorly crystalline silicotitanate analogue of pharmacosiderite,[2] over the pH range of 10−13 and a TIPT/TEOS ratio ranging from 1:4 to 1:10. The molar ratio of the final seeded product to seed crystal is approximately 80:1. Doubling or halving the seed amount did not greatly influence the crystallinity or purity of the product; and with no SNL-A seed, the desired product did not form under any attempted experimental conditions. Heating times for the synthesis of the rubidium and potassium analogues were optimized to minimize the formation of their respective, potential impurity phases. The $Rb_2TiSi_6O_{15}$ product contained a small amount of the Rb silicotitanate analogue of pharmacosiderite, even with a lengthy reaction time of 4 weeks at 230 °C. The impurity phase of the silicotitanate analogue of pharmacosiderite is also found in the synthesis of $Cs_2TiSi_6O_{15}$ if synthesis time and temperature are, respectively, too short or too high. A two-phase Rietveld refinement of the Rb silicotitanate product (see below) indicated that the pharmacosiderite was composed of less than 2 wt % of the sample. Synthesis of the $K_2TiSi_6O_{15}$ phase was optimized by reducing the reaction time to 3 days at 230 °C. From this reaction, no impurities were detected by XRD and visual inspection by optical microscope and SEM. Increased heating time resulted in the formation of a

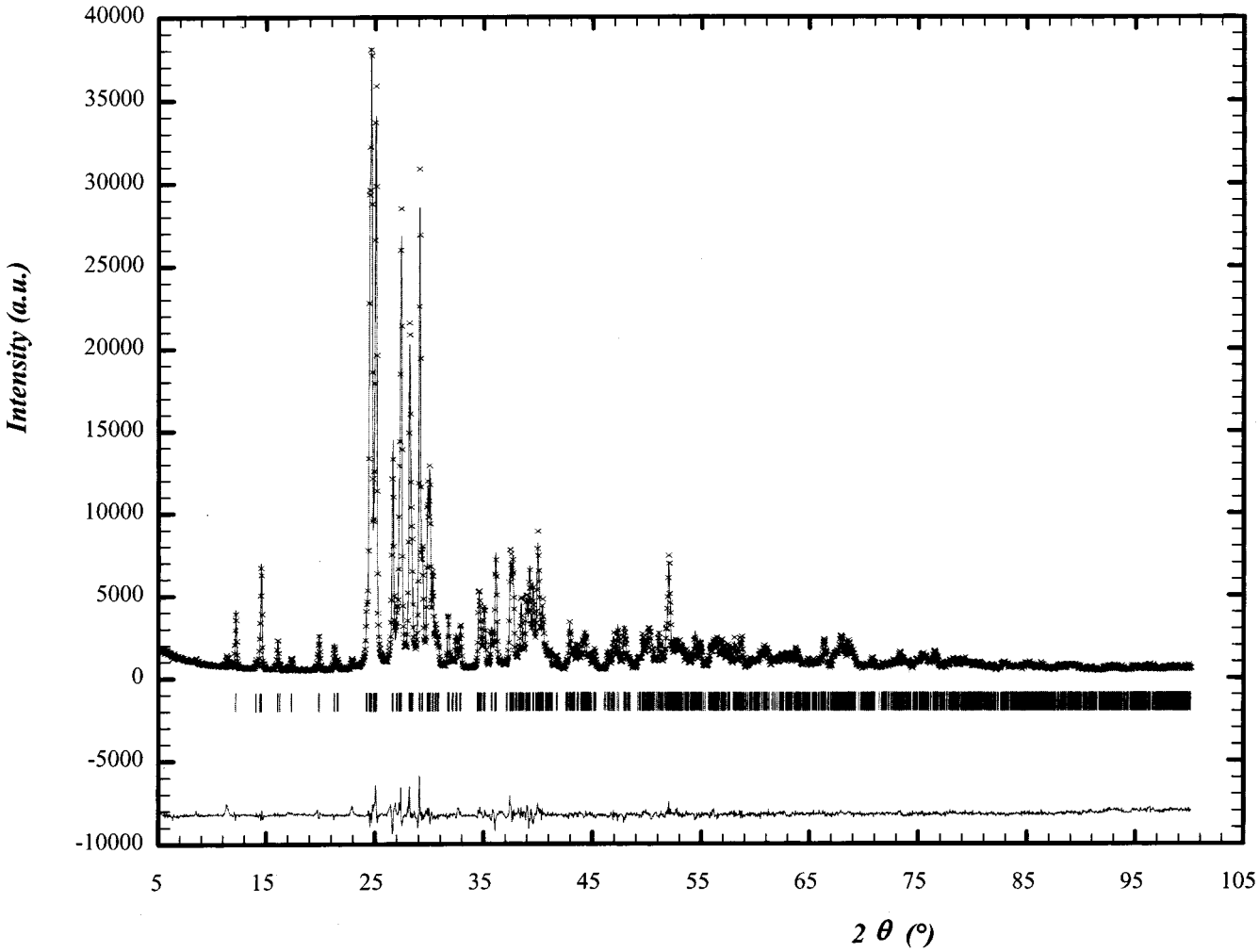

Figure 3. Observed (solid), calculated (crosses), and difference spectra of $Rb_2TiSi_6O_{15}$. The small, broad peaks in the observed pattern at $2\theta \cong 12$ and 23° correspond to a Rb silicotitanate pharmacosiderite impurity.

second phase composed of larger (50−100 μm), platelike transparent crystals that were identified by XRD to be a monoclinic ($P2_1$ #4) polymorph of $K_2TiSi_6O_{15}$, whose structure has been recently determined and reported.[27]

During the course of this work, attempts to synthesize a sodium analogue by similar seeding/hydrothermal methods failed. These attempts ranged over a variety of synthesis conditions, and reaction solution compositions predominantly produced mixtures of other phases such as quartz and ETS-4.[10]

SEM/EDS. The morphologies and stoichiometries of the Rb and K analogues were examined by SEM/EDS. Both phases have an A/Ti/Si ratio of 2:1:6 (A = Rb, K), as determined by SEM, using SNL-A as a standard.[20] The morphology of the Rb and K analogues are shown in micrographs in parts b and c of Figure 1, respectively, and are compared to that of $Cs_2TiSi_6O_{15}$ (from which their crystallization was seeded) in Figure 1a. The seeded Rb and K analogues grow in rosettelike clusters of crystals, whereas the $Cs_2TiSi_6O_{15}$ is composed of isolated crystals. The Rb and K analogues have a slightly smaller crystal size (~0.5−2 μm) than the seed crystal (~3−5 μm). The crystals of the K analogue are shaped in a tabular manner, and the crystals of the Rb and Cs analogues are irregular-shaped polyhedra.

DTA−TGA. DTA−TGA of the Rb and K analogues reveal that these materials contain only a few weight percent water, which is determined to be surface moisture, since these phases are condensed and anhydrous. There is slightly more weight loss associated with water from the Rb analogue sample, which is likely from the minor pharmacosiderite impurity, which contains both framework water as well as more surface-sorbed water. The DTA curves of the Rb and K analogues are plotted along with that of the Cs analogue in Figure 2. These analyses show a decrease in melting temperature with decreasing alkali radii (Cs > Rb > K). The melting temperatures are approximated to be 1146 °C for the Cs analogue, 1104 °C for the Rb analogue, and 1000 °C for the K analogue. None of the three phases recrystallized upon cooling nor did they undergo any phase transitions up to the melting temperature. The end products of melting are transparent glasses.

Structure Determination. Rietveld refinement using FULLPROF-98[28] software was carried out on the XRD data for $Rb_2TiSi_6O_{15}$ and $K_2TiSi_6O_{15}$, using the *Cc* (#9) solution for $Cs_2TiSi_6O_{15}$ (SNL-A) as a starting

(27) Zou, X. D.; Dadachov, M. S. *J. Solid State Chem.* **2001**, *156*, 135.

(28) Rodriguez-Carvajal, J.; Toulouse, France, 1990; p 127.

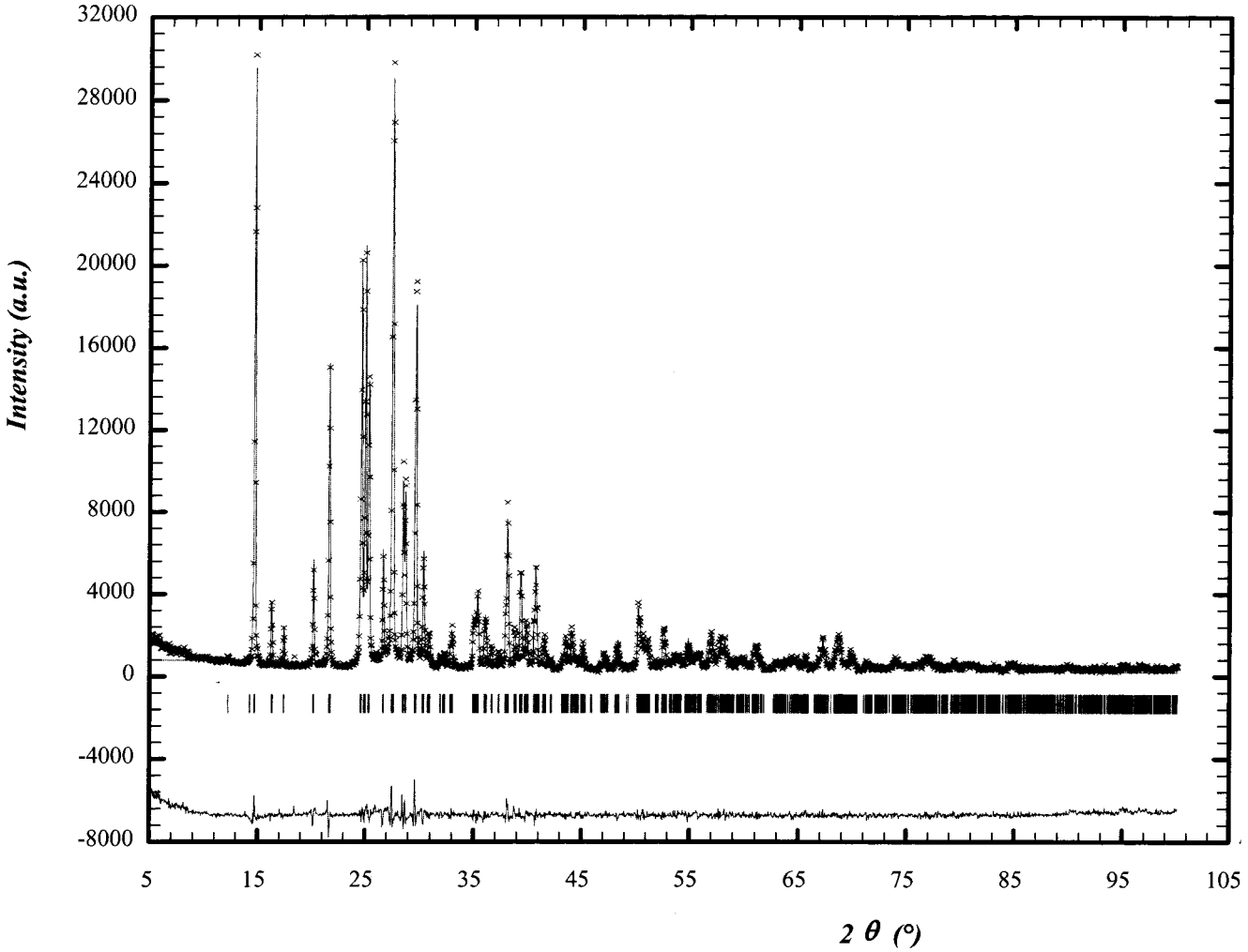

Figure 4. Observed (solid), calculated (crosses), and difference spectra of $K_2TiSi_6O_{15}$.

model.[20] Constraints were applied to the Si−O distances (1.60 ± 0.01 Å), the Ti−O distances (1.94 ± 0.025 Å) and the O−Si−O bond angles (109.5° ± 0.01°). Both phases were refined with good agreement indices (R_{Bragg} (Rb) = 3.73%, R_{Bragg} (K) = 4.35%). The crystallographic data for the Rb and K analogues are summarized in Table 1, the structural parameters are summarized in Table 2, and selected bond lengths and angles are compiled in Tables 3 and 4 for the Rb and K analogues, respectively. The observed, calculated, and difference patterns for the Rb and K analogues are shown in Figures 3 and 4, respectively. For the K analogue, no peaks were left unaccounted for by this single-phase refinement, indicating the purity of the sample.

The Rb analogue had two weak and broad peaks unaccounted for by the model at $2\theta \cong 12$ and 23°. These peak positions are approximately the same as those reported for the potassium and cesium silicotitanate analogues of pharmacosiderite.[2] Although synthesis and structural data have not been reported for the Rb silicotitanate analogue of pharmacosiderite, data are available for the potassium and cesium silicotitanate pharmacosiderite analogues, and the peak positions do not change significantly between the various ion-exchanged forms of this phase.[2] A two-phase refinement using FULLPROF[28] was performed to confirm the identity and estimate the quantity of this impurity for future calorimetry studies. Only the cell parameters and profile parameters were refined for the impurity phase, and the structural parameters were fixed on the basis of reported values.[2] The Brindley coefficient[29,30] was assumed to be essentially equal for the two phases since they are composed of the same atom types and have the same particle size, approximately. By this treatment of the X-ray data, ~1.5% of the sample is estimated to be composed of the Rb silicotitanate pharmacosiderite.

Structure Description. The overall framework and ring structures described for SNL-A[20] (*Cc*-$Cs_2TiSi_5O_{15}$) apply to the $Rb_2TiSi_6O_{15}$ and $K_2TiSi_6O_{15}$ structural analogues, and are, therefore, not described in detail in this report. The main feature of these isostructural phases is the presence of the unbranched dreier (a nomenclature term defined in the referenced work by Liebau) silicate single layers[31] that are parallel to the *xy* plane and stacked along the *z*-axis. Each layer is rotated 90° with respect to the next layer, within the *xy* plane. These silicate layers are composed of alternating rows of five- and eight-member rings of SiO_4 tetrahedra, and the layers are folded in a corrugated fashion, parallel to the long axis of the alternating rows.

(29) Hill, R. J.; Howard, C. J. *J. Appl. Crystallogr.* **1987**, *20*, 467.
(30) Brindley, G. W. *Philos. Mag.* **1945**, *36*, 347.
(31) Liebau, F.; Springer-Verlag: Berlin, 1985; p 154.

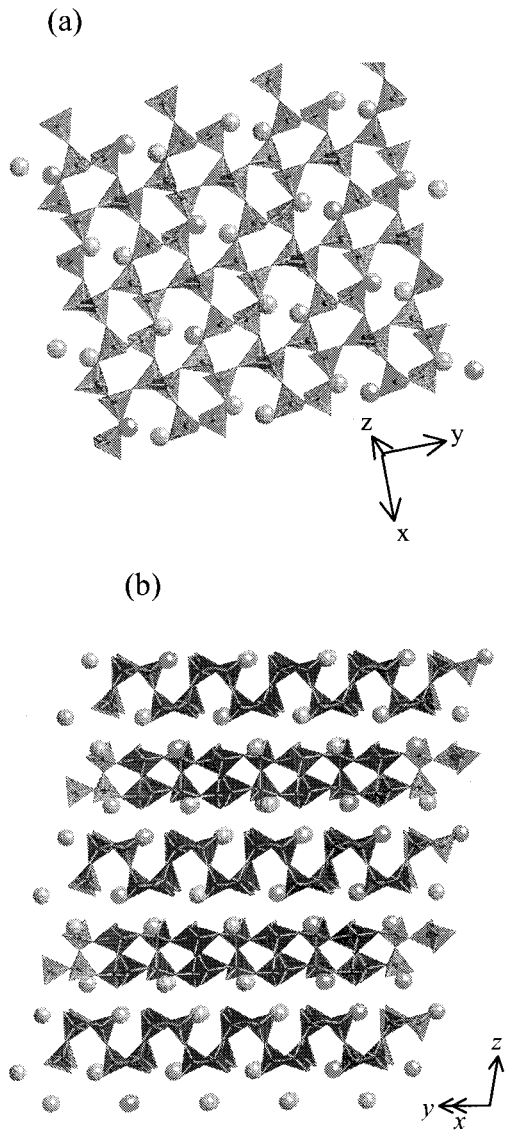

Figure 5. (a) The silicate layers of $A_2TiSi_6O_{15}$ (A = Cs, Rb, K), viewed approximately down the *z*-axis. This view shows the alternating rows of five- and eight-member rings made up of corner-sharing SiO_4 tetrahedra. (b) An edge-on view of the silicate layers, revealing the corrugated nature of these layers. The TiO_6 octahedra, which reside between the silicate layers and connect them in the *z*-direction, have been removed for ease of viewing.

Table 5. Structural Parameters and ^{29}Si NMR Data for $A_2TiSi_6O_{15}$ (A = Cs, Rb, K) Showing Correlation between *a*- and *b*-Axes and Si−O−X (X = Ti, Si) Bond Angles

alkali metal	avg ^{29}Si NMR shift (ppm)	avg Si−O−Si bond angle (deg)	avg Si−O−X bond angle (deg)[a]	*a*-axis (Å)	*b*-axis (Å)
Cs	102.4	147.1	145.4	12.998	7.501
Rb	99.0	143.9	142.21	12.736	7.339
K	98.1	141.0	140.9	12.570	7.253

[a] X = Ti, Si.

The silicate layers are viewed in parts a and b of Figure 5. Figure 5a shows the alternating rows of the five- and eight-member rings, and Figure 5b shows an edge-on view of the corrugated (folded) silicate layers. The titanium octahedra, which are removed from parts a and b of Figure 5 for ease of viewing, are located between the silicate layers, linking these layers in the *c*-direction.

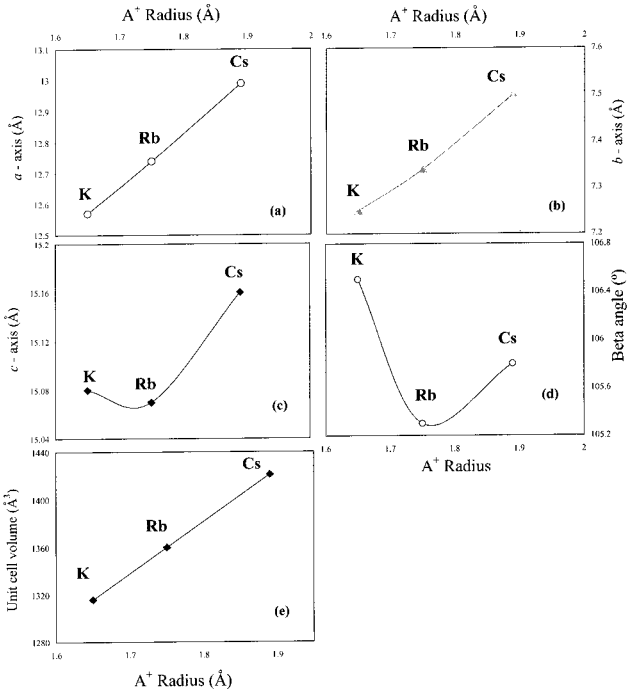

Figure 6. (a) *a*-axis, (b) *b*-axis, (c) *c*-axis, (d) β-angle, and (e) unit cell volume plotted as a function of alkali radius (Cs > Rb > K).

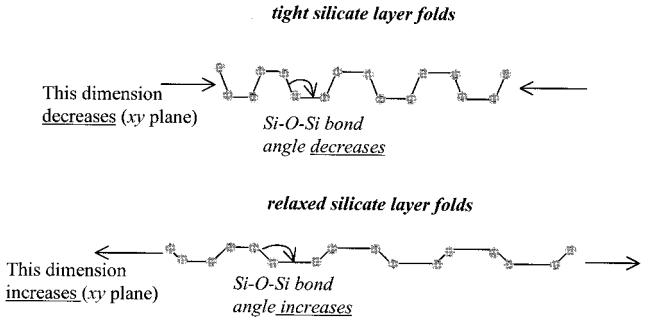

Figure 7. A schematic of the folded silicate layers of $A_2TiSi_6O_{15}$ (A = Cs, Rb, or K), illustrating the changes in unit cell dimensions and the Si−O−Si bond angles as a function of the "tightness" of the layer folds.

Table 6. Comparison of ^{29}Si NMR Shifts for $Cs_2TiSi_6O_{15}$, $Rb_2TiSi_6O_{15}$, and $K_2TiSi_6O_{15}$

$Cs_2TiSi_6O_{15}$ δ_{obs} (ppm)	$Rb_2TiSi_6O_{15}$ δ_{obs} (ppm)	$K_2TiSi_6O_{15}$ δ_{obs} (ppm)
−96.8	−94.1	−92.1
−97.8	−95.2	−96.1
−100.2	−97.7	−96.4
−102.4	−98.9	−101.3
−107.3	−101.3	−101.4
−110.0	−101.7	−102.2

The unit cell volumes, *a*-, *b*-, and *c*-axes, and β-angles are plotted as a function of alkali (Cs, Rb, K) radius[32] in Figure 6. The unit cell volume and the *a*- and *b*-axes increase linearly with increasing alkali radius (K < Rb < Cs), and there is a ~3.4% change in both the *a*- and *b*-directions. The increases in the *a*- and *b*-dimensions appear to correlate with a relaxation of the folds of the silicate layers, as illustrated in Figure 7. There is evidence for relaxation of silicate layer folds in both the X-ray structural data and ^{29}Si NMR data, and this

(32) Shannon, R. D. *Acta Crystallogr.* **1976**, *A32*, 751.

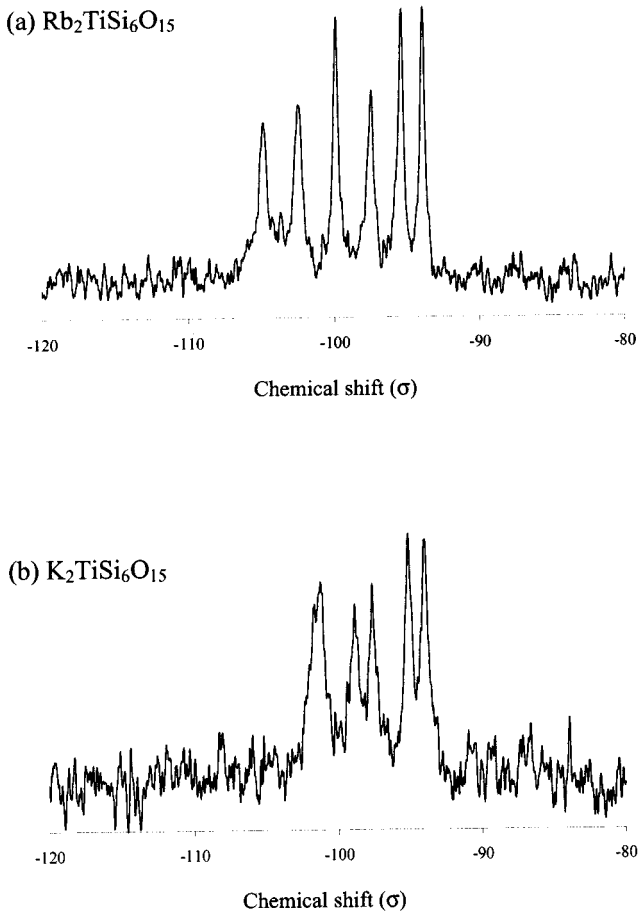

Figure 8. ^{29}Si NMR spectra of $Rb_2TiSi_6O_{15}$ (a) and $K_2TiSi_6O_{15}$ (b). Both show six peaks of approximate equal integrated intensity, which correspond with the six crystallographically unique silicon sites in the structure.

supporting data is compiled in Table 5. By the XRD data, a decrease (or tightening) of the average Si−O−Si bond angle of the Cs (147.1(0.7)°) > Rb (143.9 (0.7)°) > K (141.0 (0.7)°) analogue is observed, which correlates with the decrease in the *a*- and *b*-axes. The ^{29}Si NMR data reveals a decrease in average downfield chemical shift (Table 5), also corresponding with the decrease in alkali radii and *a*- and *b*-axes. It is a generally observed phenomenon for silicate materials that ^{29}Si NMR downfield shifts decrease as the Si−O−X (X = metal in second coordination sphere of the Si) bond angles decrease.[22,33,34] The second main contributing factor to the ^{29}Si chemical shift in the silicate-based materials is the identity of the atoms in the second coordination sphere of the SiO_4 tetrahedra. Since each of the SiO_4 tetrahedra of the $A_2TiSi_6O_{15}$ (A = Cs, Rb, K) phases are bridged to three other SiO_4 tetrahedra and one TiO_6 octahedra, ^{29}Si chemical shifts may be attributed almost entirely to the Si−O−X bond angles and related structural parameters (i.e., Si−X distance).[22] The data summarized in Table 5 together suggest that the silicate layers of $A_2TiSi_6O_{15}$ (A = K, Rb, Cs) respond in an accordion-like fashion to a change in the size of the interlayer alkali atoms, expanding the layers by relaxing the Si−O−Si bond angles with increasing alkali radius. However, the direct cause for this expansion with increased alkali radius is not entirely clear.

The *c*-axis dimension changes minimally (only ∼0.6%), and the change is not correlated with alkali radius [*c* (Cs) = 15.156, *c* (Rb) = 15.061, and *c* (K) = 15.082 Å]. Also, the average Si−O−Si bond angles of $Cs_2TiSi_6O_{15}$ and $K_2TiSi_6O_{15}$ are, respectively, larger and smaller than 143° (the average Si−O−Si bond angle in silicates);[22,35] this suggests that the silicate layers of the Cs analogue and K analogue might be somewhat strained.

The ^{29}Si MAS NMR spectra of the Rb analogue and the K analogue are shown in parts a and b of Figure 8, respectively. Like the Cs analogue, each has six peaks of approximately equal integrated intensity, one for each crystallographically unique Si site in the structure. This again confirms that the noncentrosymmetric *Cc* space group solution is correct for these phases, rather than the centrosymmetric *C*2/*c* space group, which would show three unique silicon sites by NMR.[20] The ^{29}Si chemical shifts for the Rb and K analogues are summarized in Table 6, along with those for the Cs analogue for comparison. Like the Cs analogue, there is a broad range of Si−O−X (X = Si, Ti) angles observed by XRD data for the Rb- and K analogues, and this range is directly reflected in the large range of chemical shifts for all Q^3 (bonded to three Si and one Ti each) SiO_4 tetrahedral sites. Average Q^3 chemical shifts for silicotitanates usually range approximately from −96 to −105 ppm.[36]

We do not observe the silicotitanate pharmacosiderite peak at $\sigma \sim -88$ ppm in the ^{29}Si direct NMR spectrum of $Rb_2TiSi_6O_{15}$. However, we believe that this NMR result is in agreement with the two-phase refinement of this sample, which shows ∼1.5% pharmacosiderite. The Rb analogue cannot be synthesized without this small impurity phase, and it cannot be easily separated after synthesis. When a ^{29}Si CP NMR (cross polarization) experiment is performed instead of the direct NMR experiment, we do observe a small pharmacosiderite peak. This is explained by the cross-polarization enhancement of the pharmacosiderite Si signal, which is due to the close proximity the Si nuclei to protons contained in framework OH and channel H_2O. In contrast, the condensed $Rb_2TiSi_6O_{15}$ phase contains no OH^- or H_2O in its framework, and therefore the intensity of its Si NMR peaks is not enhanced by the cross-polarization experiment.

Summary and Conclusions

In this report, we have presented the synthesis and characterization of $Rb_2TiSi_6O_{15}$ and $K_2TiSi_6O_{15}$, structural analogues of SNL-A (*Cc*-$Cs_2TiSi_6O_{15}$). By combined hydrothermal and seeding methods, we have obtained materials that we were unable to otherwise synthesize in a pure, crystalline form. Particularly, by seeding methods, we were able to synthesize the first reported, rubidium silicotitanate phase, $Rb_2TiSi_6O_{15}$. The K analogue, $K_2TiSi_6O_{15}$, was obtained in an extremely pure

(33) Couty, R.; Gernandez, L. *C. R. Acad. Sci., Ser. IIa: Sci. Terre Planetes* **1996**, *323*, 919.
(34) Johnson, G. M.; Mead, P. J.; Dann, S. E.; Weller, M. T. *J. Phys. Chem. B* **2000**, *104*, 1454.
(35) Gibbs, G. V. *Am. Mineral.* **1982**, *62*, 421.
(36) Balmer, M. L.; Bunker, B. C.; Wang, L. Q.; Peden, C. H. F.; Su, Y. *J. Phys. Chem. B* **1997**, *101*, 9170.

form, and $Rb_2TiSi_6O_{15}$ contained only a minor silicotitanate pharmacosiderite impurity. Both were synthesized in approximately 90% yield based on TIPT, the limiting reagent of the reaction. The K and Rb analogues were characterized by Rietveld refinement of powder XRD data, SEM/EDS, TGA−DTA, and ^{29}Si NMR. We observed direct correlation of alkali radius (Cs > Rb > K) with: (1) melting temperature and (2) unit cell parameters including volume (Å^3), *a*-axis, and *b*-axis (Å). The increasing *a*- and *b*-axes with increasing alkali radius can be correlated with a relaxation of the silicate layer folds, which is also noted by an increase in average Si−O−Si bond angle. The increase in Si−O−Si bond angle is also evidenced by an increased downfield shift of the average ^{29}Si NMR peak position. The *c*-axis and β-angle change minimally with alkali radius and do not follow any predictable trends.

In addition to their potential application as durable ceramic waste form materials,[24,25] these new isostructural phases (and their polymorphic forms)[37] have presented the opportunity to relate phase stability to properties such as framework structure and chemical composition to structurally complex, ternary, and quaternary oxide phases. Therefore, this work and related works provide an important stepping stone toward the tailoring of materials with optimized properties such as chemical durability and thermodynamic stability.

Ongoing research involving calorimetry investigations and density functional theory calculations will be used to guide our understanding of trends in thermodynamic stability with varying alkali composition. Finally, synthesis, characterization, and calorimetry studies of mixed alkali phases $(A_xA'_{1-x})_2TiSi_6O_{15}$ (A = Cs, Rb, K, Na) are also currently underway.

Acknowledgment. Sandia (T.M.N., F.B., and M.N.) is a multiprogram laboratory operated by Sandia Corporation, a Lockheed Martin Company, for the U.S. Department of Energy under Contract No. DE-AC04-94AL85000. M.N. and T.M.N. thank the DOE Environmental Management Science Program (EMSP) for funding for this work. The NMR work (R.S.M.) was performed under the auspices of the U.S. Department of Energy by University of California Lawrence Livermore National Laboratory under Contract No. W-7405-Eng-48.

CM0102943

(37) Grey, I. E.; Roth, R. S.; Balmer, M. L. *J. Solid State Chem.* **1997**, *131*, 38.